Numerical Investigation of Unsteady Inlet Flowfields

T. Hsieh,* A.B. Wardlaw Jr.,* and P. Collins†
Naval Surface Weapons Center, Silver Spring, Maryland
and
T. Coakley‡
NASA Ames Research Center, Moffett Field, California

The flowfield within an unsteady two-dimensional inlet is studied numerically, using a two-dimensional Navier Stokes and a one-dimensional inviscid model. Unsteadiness is introduced by varying the outflow pressure boundary condition. The cases considered include outflow pressure variations that were a single pressure pulse, a rapid increase, and a small-amplitude sine function. The amplitude of the imposed exit plane pressure disturbance varied between 1 and 14% of the mean exit pressure. At the higher levels of pressure fluctuation, the viscous flowfield results bore little resemblance to the inviscid ones. The viscous solution included such phenomena as shock trains, bifurcating separation pockets, and disappearing and reforming terminal shocks and separation pockets.

I. Introduction

RECENT tests of integral rocket/ramjet propulsion systems have exhibited undesirable, high-amplitude pressure fluctuations caused by the ramjet combustor.[1-3] The most troublesome oscillations are in the frequency range of 100-500 Hz and the corresponding root-mean-square pressure oscillation amplitudes can reach up to 20% of the mean combustor pressure. Inlet/combustor interaction is one of the sources that may enhance the pressure oscillations for the entire propulsion system. This paper is motivated by the need to better understand the response of the inlet, particularly the terminal shock to combustor-induced pressure oscillations. To accomplish this, only the diffuser portion of the inlet is considered, which is consistent with the experimental configuration used in Refs. 12-15. Both inviscid and viscous models are applied.

Most existing analyses of the inlet are based on asymptotic solutions to inviscid models[4-6] or acoustic plus quasisteady shock methods.[7] In these treatments, the viscous effects are accounted for through an inviscid-viscous approach or an effective configuration that simulates boundary-layer displacement. The predictions of such models are in good agreement with experiment in special cases of small-amplitude oscillations in inlets with little or no separation. In other situations, these approaches omit relevant physical phenomena and are, therefore, suspect. In this paper, the Navier-Stokes equations are applied to the study of inlets featuring large-amplitude fluctuations and significant separation regions. Successful application of numerical procedures for solving the Navier-Stokes equations in unsteady inlets have been reported in Refs. 8-10. However, these papers consider only the inlet with low-amplitude fluctuations. In this paper, the viability of numerically solving the Navier-Stokes equations for two-dimensional inlets with large-amplitude disturbances is demonstrated. Two types of unsteady outflow boundary conditions are considered: a pressure pulse and a rapid increase in exit pressure. The resulting flowfields exhibit complex phenomena such as shock trains, disappearing and reforming terminal shocks, and bifurcating separation pockets. Unfortunately, experimental data are not available to check the accuracy of the calculations. Nevertheless, these computations suggest the type of flowfield structures that are likely to occur in a highly unsteady inlet.

In addition to the viscous model, a one-dimensional inviscid model is applied to the unsteady inlet. This serves to indicate the differences between a model including viscous, two-dimensional effects and one that does not. The one-dimensional inviscid model has also been applied to cases of small-amplitude forced periodic oscillation of pressure at the exit plane and compared with experimental data.

In Sec. II the viscous and inviscid numerical procedures are outlined. Results for steady and unsteady calculations are given in Sec. III, while a summary is provided in Sec. IV.

II. Numerical Procedures

Inviscid Model

The one-dimensional unsteady Euler equations describing flow in an inlet, written in conservation forms are

$$\frac{\partial \rho A}{\partial t}+\frac{\partial \rho u A}{\partial x}=0$$

$$\frac{\partial \rho u A}{\partial t}+\frac{\partial}{\partial x}[(\rho u^2+p)A]=pA_x$$

$$\frac{\partial}{\partial t}\left[\rho\left(e+\frac{u^2}{2}\right)A\right]+\frac{\partial}{\partial x}\left\{\left[\rho\left(e+\frac{u^2}{2}\right)+p\right]uA\right\}=0 \quad (1)$$

where A, ρ, p, u, and e are the duct cross-sectional area, density, pressure, velocity, and internal energy, respectively. These equations have been solved in finite-difference form using the second-order time-accurate MacCormack scheme. When a normal shock exists within the duct, it is fitted. The equations for fitting the shock arise from the single admissable characteristic equation and the Rankine-Hugoniot relations. The computation is done using a transformation that maps the shock onto the same coordinate line in each time step. The inflow and outflow boundaries are prescribed in accordance with characteristic theory. At the inflow, the flow is presumed to be supersonic and ρ, u, and e are specified, while at the outflow the Mach number is less than one and only pressure is prescribed.

Presented in part as AIAA Paper 84-0031 at the AIAA 22nd Aerospace Science Meeting, Reno, NV, Jan. 9-12, 1984; received Nov. 15, 1985; revision received May 23, 1986.

*Aerospace Engineer. Associate Fellow AIAA.
†Mechanical Engineer.
‡Research Scientist. Member AIAA.

Navier-Stokes Model

The numerical method used for solving the Navier-Stokes equations is described in Refs. 8 or 10. The governing equations are the time-dependent, mass-averaged, thin-layer Navier-Stokes equations for compressible flow that are written in conservation form. A general coordinate transformation is used to map the physical plane into a rectangular computational one. A modified version of MacCormack's hybrid method[11] is applied using the finite-volume approach. Total temperature and pressure are specified at the inflow boundary, while static pressure is defined at the outflow boundary. Along the upper and lower walls of the inlet, no-slip boundary conditions are applied in conjunction with adiabatic wall conditions. These conditions are more fully discussed in Ref. 8. The k-ω^2, the two-equation eddy viscosity model by Wilcox and Rubesin,[17] is applied using the set of constants described in Ref. 10.

All calculations for the viscous model were carried out on a mesh with 80 points in the longitudinal direction and 50 points in the vertical direction. The mesh was exponentially stretched in the vertical direction near the upper and lower duct walls in a manner that assured the presence of at least two points in the laminar sublayer. The longitudinal mesh points were clustered in the diffuser region (i.e., between $x/H=1$ and 3) in order to improve the resolution of the terminal shock.

The initial flowfield was prescribed using the one-dimensional steady duct solution. Near the upper and lower walls, flow properties were modified to account for the boundary layer using the one-seventh power law along with a linear laminar sublayer profile for the viscous model. Appropriate initial profiles for k and ω^2 were also implemented.

The computational method proved to be very robust and provided solution to all of the sets of boundary conditions specified with little difficulty. The calculations were performed on the NASA-ARC-Cray/XMP computer and used 3.6×10^{-4} CPU s/mesh-point/time step.

III. Results and Discussion

The inlet configuration considered in this paper is depicted in Fig. 1 and has been experimentally investigated by Sajben et al.[12-15] A detailed description of it is given in Ref. 12. Denoting the ratio of the exit plane to the reservoir pressure as R and the reservoir pressure as p_t, the calculated cases can be summarized as follows: 1) inviscid and viscous steady flow for R values of 0.72, 0.82, and 0.862; 2) inviscid unsteady flow with small-amplitude, periodic exit plane perturbation about average R values of 0.72 and 0.82; 3) inviscid and viscous unsteady flow with a rapid change in exit pressure from $R=0.72$-0.82; and 4) inviscid and viscous unsteady flow in response to a single exit pressure pulse of amplitude $\Delta p/p_t=0.1$ at $R=0.72$. The amplitude of exit plane pressure variation was 1.2% in case 2 and 14% in cases 3 and 4. In the remainder of this section, these cases are discussed in order. The experimental results taken by Sajben are applicable to the first two cases only.

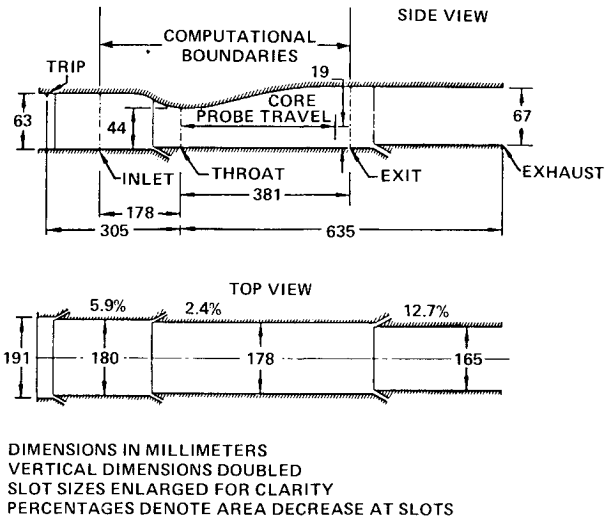

Fig. 1 Inlet-diffuser configuration (courtesy of Sajben).

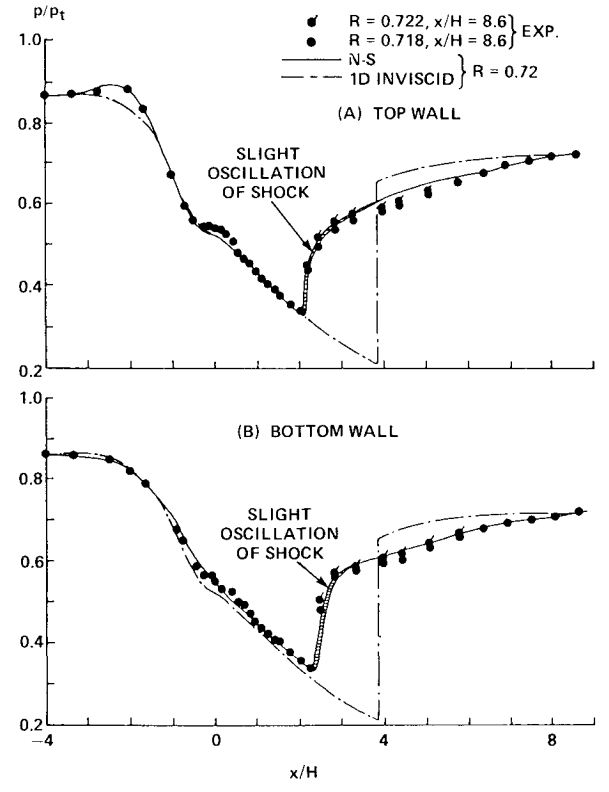

Fig. 2 Calculated and experimental wall pressures at nominal R of 0.72.

Steady Flow

For verification purposes computations have been carried out in the case of steady flow with R values of 0.72, 0.82, and 0.862. Results are compared to experiment in Figs. 2-4. The calculations were set up with the inflow and outflow boundaries located at $x/H=-4$ and 8.6. Here x is the axial distance along the inlet, H is the throat height, and $x=0$ occurs at the throat. As is shown in Fig. 1, the actual inlet extended from $x/H=-6.93$-14.43 and featured three suction slots along the bottom of the inlet that were not simulated in the calculation.

The results for $R=0.72$ are shown in Fig. 2. Here two sets of experimental measurements are available at slightly different values of R. These results are nearly identical except in the vicinity of the shock, where a small difference occurs as indicated in Fig. 2. The calculated results are in good agreement with the experiment. In the vicinity of the shock, the solution oscillates slightly, as is shown by the shaded region, and does not achieve a steady state. This case turns out to be a self-excited oscillation of the terminal shock[15,16] and will be reported separately.

Figure 3 illustrates results for an R value near 0.82. Here three sets of experimental data are available for slightly different values of R and the results differ noticeably in the immediate vicinity of the shock. The calculated wall pressure is in reasonable agreement with measurements.

Two sets of measured wall pressures at a nominal R value of 0.862 are shown in Fig. 4. These results illustrate the sensitivity of small perturbations in the exit pressure on the wall pressure, particularly in the immediate vicinity of the throat.

Here calculated results are seen to agree well with only one set of experimental data.

The viscous results provided in Figs. 2-4 appear to be in reasonable agreement with the experiment, despite the possible influence of three-dimensionality on the experimental results. Unfortunately, the same cannot be said for the one-dimensional inviscid results also shown in these figures. Here large differences are seen in the wall pressure near the throat, with the inviscid solution mispositioning the shock. At $R=0.862$, the inviscid flowfield predicts a terminal shock, while experiment and the Navier-Stokes solution feature a completely subsonic inlet.

The results of velocity distribution across the inlet at six stations for $R=0.82$ are shown in Fig. 5. The agreement with experiment is excellent for the bottom wall. For the top wall, the solution slightly underpredicts the velocity. Similar results for $R=0.72$ are shown in Fig. 6. As shown in Figs. 6a-6c, strong flow separation occurs on the top wall. The solution accurately predicts the length of the separation pocket, but underpredicts the thickness (Figs. 6a-6c), with the zero velocity located about halfway between the wall and the experimental data. There is no flow separation on the bottom wall and the agreement between the solution and the experiment is satisfactory. On the downstream side of the separation pocket (Figs. 6e and 6f), the experiment indicates a fully developed channel flow, as the boundary layer from both walls join together, before the exit plane, and yet the solution indicates that there is still an inviscid core at the exit plane.

From the above comparison, it is clear that the numerical solution provides a correct qualitative prediction of the inlet flowfield. However, aspects of the flow such as the separation pocket thickness are not accurately described.

Inviscid, Small-Amplitude Periodic Oscillations

The examples selected for investigation are the forced oscillation experiments reported in Ref. 13. These tests were conducted at R values of 0.82 and 0.72, using a downstream

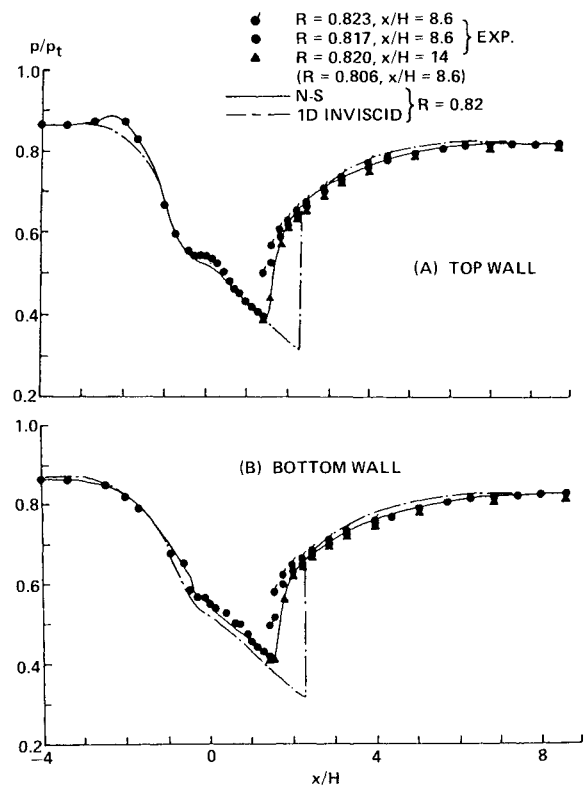

Fig. 3 Calculated and experimental wall pressures at nominal R of 0.82.

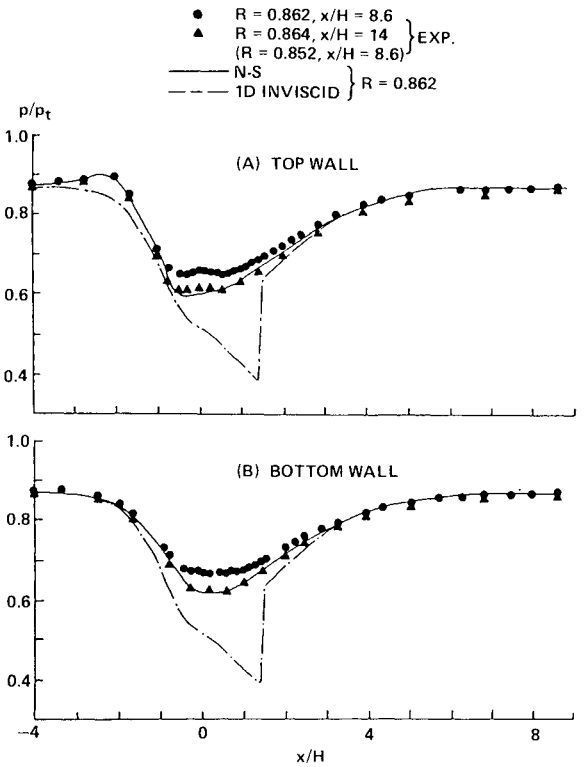

Fig. 4 Calculated and experimental wall pressures at nominal R of 0.862.

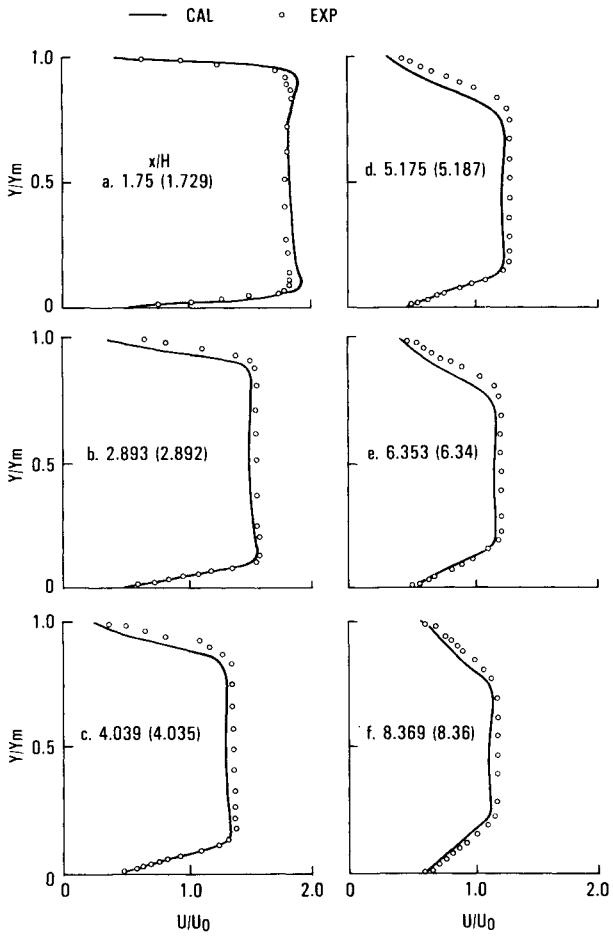

Fig. 5 Comparison of calculated and measured axial velocity profiles, $R=0.82$.

pressure fluctuation on the order of 1%. Tests conducted at $R=0.82$ produced a weak terminal shock that induced little flow separation, while experiments carried out at $R=0.72$ featured a stronger terminal shock that induced significant downstream flow separation. The Navier-Stokes model considered in this paper has been applied to this case in Ref. 9. The Navier-Stokes results are in reasonable agreement with experiment for both the strong and weak terminal shock cases. The predictions obtained by applying the inviscid, one-dimensional model to these cases are shown in Figs. 7 and 8. Here R values of 0.867 and 0.843 were used in place of the experimentally measured ones of 0.82 and 0.72, respectively. As indicated in Figs. 2 and 3, application of the measured exit pressure incorrectly locates the shock. The selected R values produced the measured Mach number upstream of the shock. Here the downstream pressure variation was set at the amplitude of the first harmonic experimentally measured at the exit plane. Predicted fluctuations were compared to the first harmonic of the measured property oscillations. The weak shock results agree well with experiment, while the strong shock predictions did not. This suggests that in cases with sizable separation regions an inviscid model is not adequate.

Inlet Response to an Increase in Exit Pressure

The response of an inlet to a rapid increase of exit pressure, which is shown in Fig. 9a, has been computed for an R value increase from 0.72 to 0.82 (14% increase) in 0.2 ms. Both inviscid and viscous models were applied. The inviscid model took 800 steps to arrive at steady state, while the viscous one took 2800 steps. The pressure-time history for the inviscid model is shown in Fig. 10. After the application of the exit pressure increase, a pressure wave moves upstream. When it reaches the terminal shock, it pushes the shock upstream past the final equilibrium position slightly.

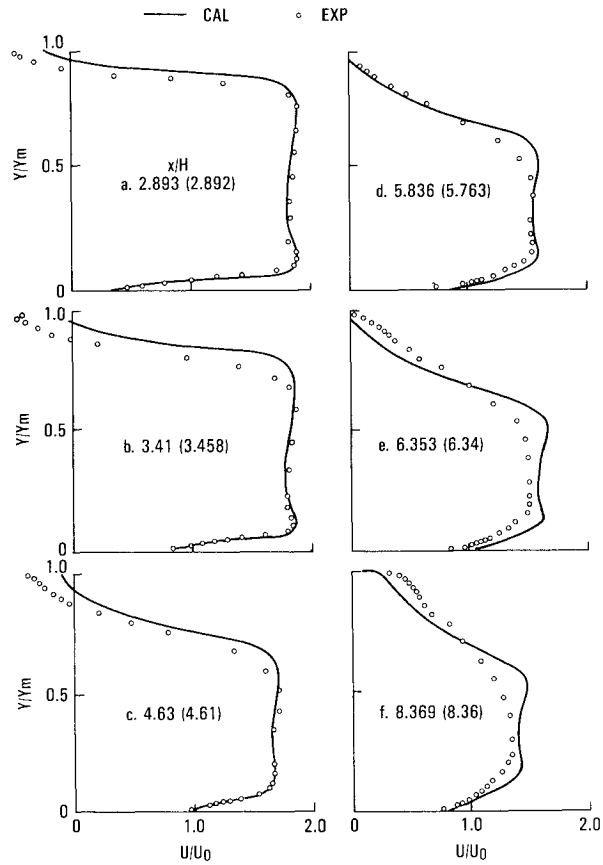

Fig. 6 Comparison of calculated and measured axial velocity profiles, $R=0.72$.

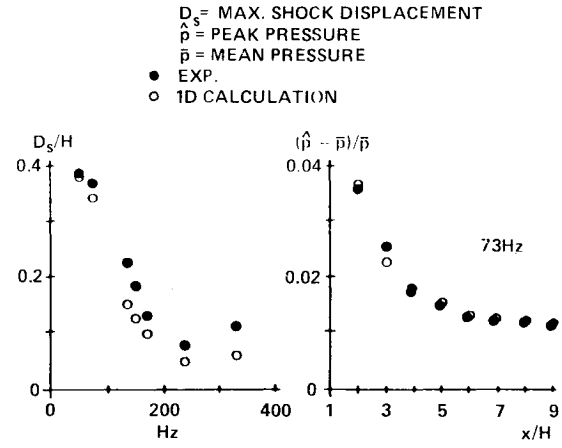

Fig. 7 Comparison of one-dimensional inviscid predictions with experiment for the weak shock case, $R=0.82$.

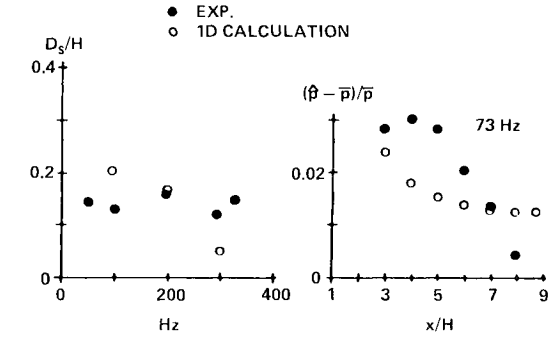

Fig. 8 Comparison of one-dimensional inviscid prediction with experiment for the strong shock case, $R=0.72$.

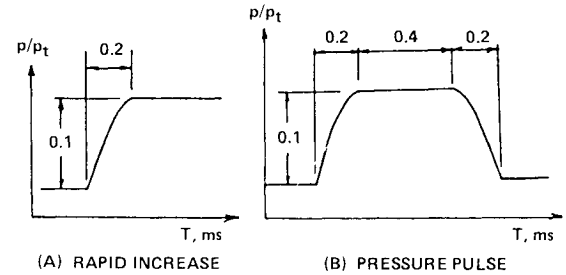

Fig. 9 Exit pressure variation as a function of time.

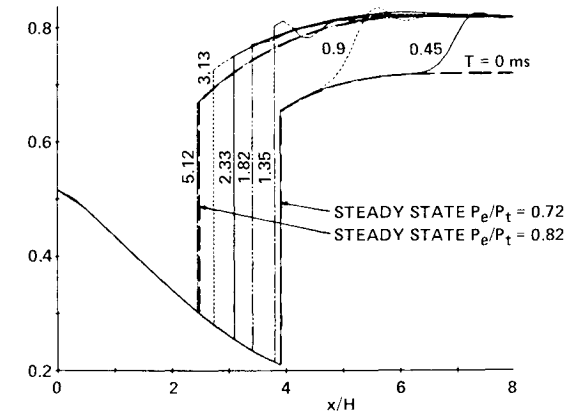

Fig. 10 Pressure history and shock motion in response to a rapid increase in exit pressure calculated by the one-dimensional inviscid models.

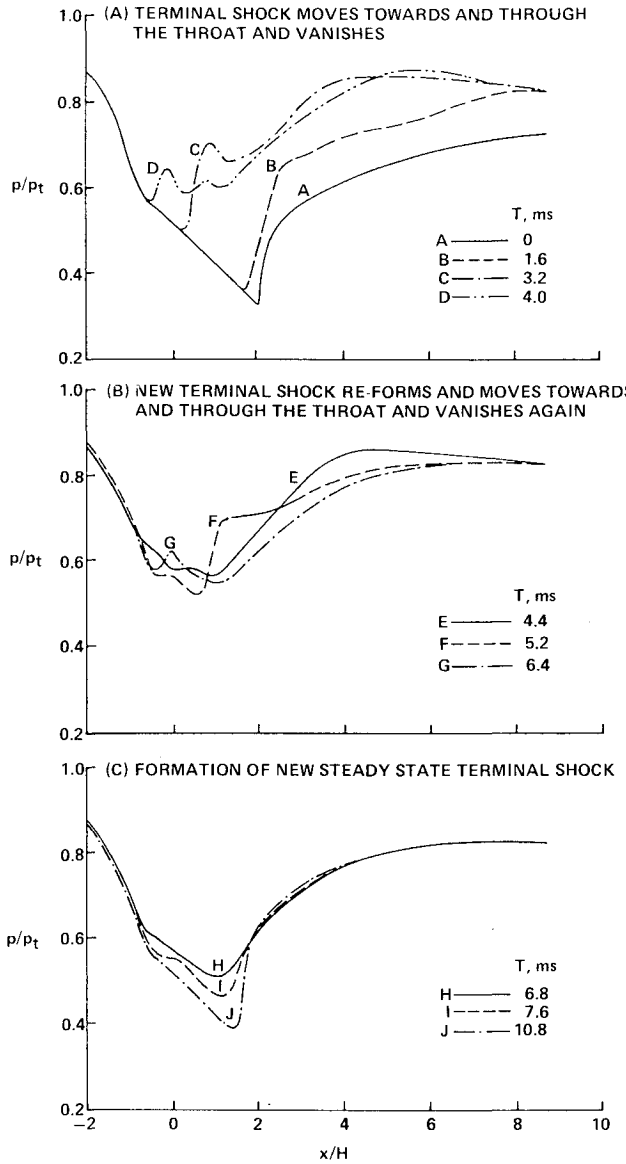

Fig. 11 Pressure history and shock motion in response to rapid increase of exit pressure from $R=0.72$–0.82 calculated using the Navier-Stokes model.

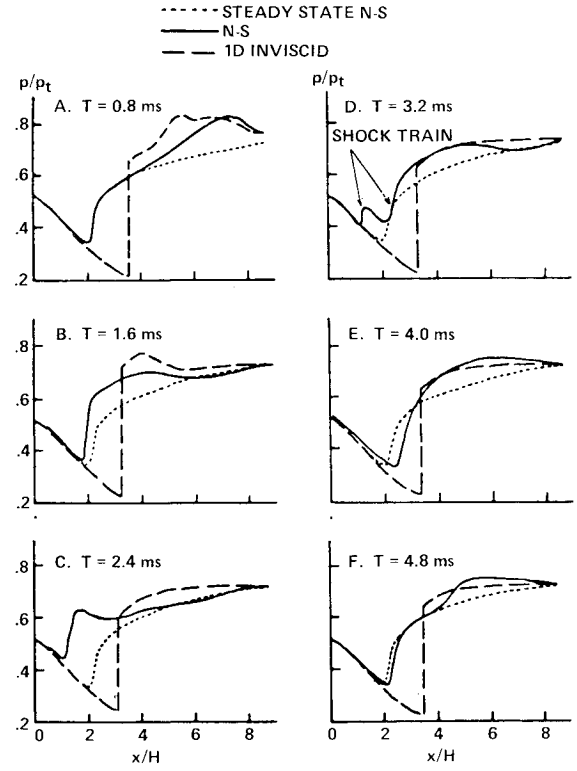

Fig. 12 Top wall pressure history and unsteady shock motion due to pressure pulse applied at exit, $R=0.72$, $\Delta p/p_t=0.1$.

The shock location then gradually relaxes back to the new steady-state location. In the viscous model, the terminal shock behaves in a much more complex manner, as can be seen from the pressure-time history shown in Fig. 11. The terminal shock moves toward and through the throat, becomes weaker (Fig. 11a, curves A–D) and vanishes at $T=4.4$ ms (Fig. 11b, curve E), leaving a subcritical inlet. A new terminal shock reforms at $T=5.2$ ms and moves toward and through the throat (Fig. 11b, curves E and G), vanishing again at $T=6.8$ ms (Fig. 11c, curve H). The transient motion of the second terminal shock occurs throughout a subcritical inlet. The final terminal shock slowly forms and settles at the new steady-state location shown in Fig. 11c.

Inlet Response to a Pressure Pulse

A single pressure pulse, which is shown in Fig. 9b and has a magnitude of 14% of the mean exit pressure, was applied to an inlet with $R=0.72$. The pulse consisted of an amplitude $\Delta p/p_t=0.1$ wave with a rise time of 0.2 ms, a duration of 0.4 ms, and a recession time of 0.2 ms. Both an inviscid and a viscous calculation were performed for this example. Calculations started with the onset of the pressure pulse and terminated when the flow was approaching steady state. The unsteady pressure variation for both of these cases is illustrated in Fig. 12, while a Mach number contour plot of the Navier-Stokes solution is shown in Fig. 13. Following the application of the unsteady pressure pulse to the inlet exit, a pressure wave moves up the inlet and interacts with the terminal shock. In the inviscid model, the shock moves toward the throat slightly and then returns to its equilibrium position. The original pulse does not strongly reflect off the shock. In the viscous case, the top wall separation lengthens and then shrinks in response to the passing of the pressure wave, as is shown in Figs. 13a–13c. The broken line near the top and bottom of the walls indicates the zero velocity line that marks the extent of the separation pocket, while the dotted line indicates the sonic line. The shock responds to the pressure wave by moving toward the throat and becoming weaker. Unlike the case discussed in the previous subsection, the terminal shock does not move through the throat. The top wall separation pocket bifurcates with one pocket visible slightly downstream of the shock and a second near the inlet exit (see Fig. 13d). A second shock forms behind the first, producing a shock train that is visible in both Figs. 13e and 12d. At this point, only a small separation pocket is left in the duct. Now the forward shock of the shock train moves through the throat and finally disappears. This leaves a single shock in the nozzle, which is located slightly downstream of the steady-state shock position. It gradually moves back to its original location and the single separation pocket present at the start of the calculation is reformed (see Fig. 13f). In Fig. 13, it can be seen that the interaction among the shock wave, separation pocket, and pulse becomes quite complicated in the viscous case.

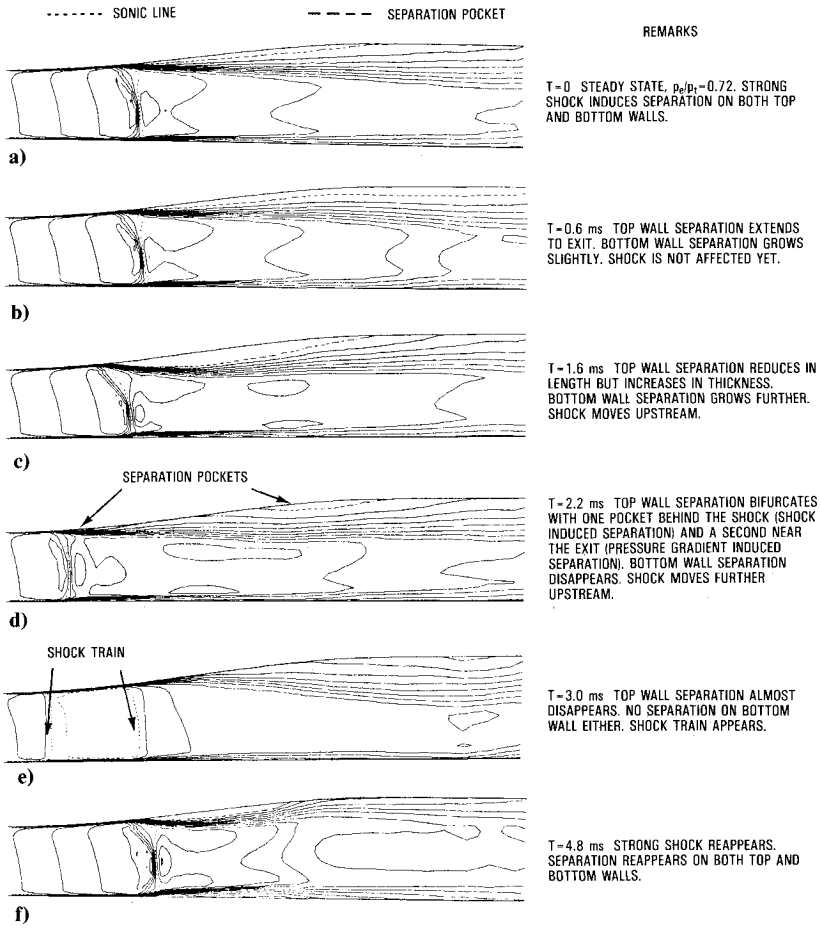

Fig. 13 Separation characteristics of diffuser flow in response to exit pressure pulse.

IV. Conclusions

Unsteady flow calculations have been performed for a two-dimensional inlet using a one-dimensional inviscid model with shock tracking and a two-dimensional Navier-Stokes approach. The unsteady cases calculated using the later method were performed with exit plane pressure variations on the order of 14% of the mean static pressure. The resulting flowfield contained a number of notable features:

1) Curved terminal shocks that disappeared and reformed as the unsteadiness progressed.

2) More than one normal shock coexisting in the inlet at once.

3) Separation region formation, bifurcation, and disappearance.

These flowfields appear to be plausible; however, the accuracy of the calculation remains to be determined, since experimental data are not available for comparison.

Comparison of the one-dimensional inviscid model with experimental data produced good agreement in one case featuring low-amplitude oscillations and weak terminal shock with little flow separation. In a similar case containing a strong shock with larger areas of flow separation, the predicted results were not in good agreement with experiment. The one-dimensional inviscid model and the Navier-Stokes approach were compared on two large-amplitude disturbance cases that featured a rapid increase in the downstream pressure and a single pressure pulse prescribed at the exit plane. In both situations, the inviscid model predicted a much simpler flowfield than that calculated by the viscous model. The inviscid flowfield essentially consisted of relatively smooth shock motion with little overshoot or oscillation. By contrast, the viscous flowfield contained a complex array of phenomena.

Acknowledgment

The work is partly sponsored by Naval Weapons Center and monitored by Dr. W. C. Clark. The computer time for the viscous calculation is provided by the Applied Computational Aerodynamics Branch of NASA Ames Research Center through a cooperation program with NSWC. We would also like to thank Eva Pegot of Experimental Fluid Dynamics Branch of NASA ARC for her assistance in making computer plots.

References

[1]Rogers, T., "Ramjet Inlet/Combustor Pulsations Study," Naval Weapons Center, China Lake, CA, NWC TP 6053, Jan. 1980.

[2]Rogers, T., "Ramjet Inlet/Combustor Analysis and Test," Naval Weapons Center, China Lake, CA, NWC T 6155, Feb. 1980.

[3]Clark, W.H., "Experimental Investigation of Pressure Oscillations in a Solid Dump Ramjet Combustor," *Journal of Spacecraft and Rockets,* Vol. 19, Jan.-Feb. 1982, pp. 47-53.

[4]Richey, G.K. and Adamson, T.C. Jr., "Analysis of Unsteady Transonic Channel Flow with Shock Waves," *AIAA Journal,* Vol. 14, Aug. 1978, pp. 1240-1247.

[5]Adamson, T.C. Jr., Messiter, A.F., and Liou, M.S., "Large Amplitude Shock Wave Motion in Two-Dimensional Transonic Channel Flows," *AIAA Journal,* Vol. 16, Dec. 1978, pp. 1240-1247.

[6]Liou, M.S. and Sajben, M., "Analysis of Unsteady Viscous Transonic Flow with a Shock Wave in a Two-Dimensional Channel," AIAA Paper 80-0195, 1980.

[7]Culick, F.E.C. and Rogers, T., "Modeling of Pressure Oscillations in Ramjets," AIAA Paper 80-1192, 1980.

[8]Coakley, T.J. and Bergmann, M.Y., "Effects of Turbulence Model Selection on the Prediction of Complex Aerodynamic Flows," AIAA Paper 79-0070, 1979.

[9]Liou, M.S., Coakley, T.J., and Bergmann, M.Y., "Numerical Simulation of Transonic Flows in Diffusers," AIAA Paper 81-1240, June 1981.

[10]Liou, M.S. and Coakley, T.J., "Numerical Simulations of Unsteady Transonic Flow in Diffuser," *AIAA Journal,* Vol. 22, Aug. 1984, pp. 1139-1145.

[11]MacCormack, R.W., "An Efficient Numerical Method for Solving the Time-Dependent Compressible Navier-Stokes Equations at High Reynolds Number," *Computing in Applied Mechanics,* Vol. 18. ASME, AMD, New York, 1976.

[12]Sajben, M., Bogar, T.J., and Kroutil, J.C., "Forced Oscillation Experiments in Supercritical Diffuser Flows with Applications to Ramjet Instabilities, "AIAA Paper 81-1487, 1981.

[13]Bogar, T.J., Sajben, M., and Kroutil, J.C., "Characteristic Frequencies of Transonic Diffuser Flow Oscillations, AIAA *Journal,* Vol. 21, Sept. 1983, pp. 1232-1240.

[14]Salmon, J.T., Bogar, T.J., and Sajben, M., "Laser Velocimeter Measurements in Unsteady, Separated, Transonic Diffuser Flows," AIAA Paper 81-1197, 1981.

[15]Bogar, T.J., "Structure of Self-Excited Oscillations in Transonic Diffusor Flows," AIAA Paper 84-1636, June, 1984.

[16]Hsieh, T., Bogar, T.J. and Coakley, T.J., "Numerical Simulation and Comparison with Experiment for Self-Excited Oscillations in a Diffuser Flow," AIAA Paper 85-1475, July 1985.

[17]Wilcox, D.C. and Rubesin, M.W., "Progress in Turbulence Modeling for Complex Flow Fields Including Effects of Compressibility," NASA TP 1517, 1980.